Chinese Journal of Chemical Engineering 28 (2020) 2099–2110

Contents lists available at ScienceDirect

Chinese Journal of Chemical Engineering

journal homepage: www.elsevier.com/locate/CJChE

Article

# Modeling the rate of corrosion of carbon steel using activated diethanolamine solutions for $CO_2$ absorption

Lubna Ghalib [1], Ahmed Abdulkareem [2], Brahim Si Ali [3], Shaukat Ali Mazari [4,*]

[1] Materials Engineering Department, Mustansiriyah University, Baghdad 14022, Iraq
[2] Mathematics Science, Directorate General of Education Rusafa 1, Baghdad, Iraq
[3] Department of Chemical Engineering, University of Malaya, 50603 Kuala Lumpur, Malaysia
[4] Department of Chemical Engineering, Dawood University of Engineering and Technology, Karachi 74800, Pakistan

ARTICLE INFO

*Article history:*
Received 20 August 2019
Received in revised form 9 February 2020
Accepted 11 March 2020
Available online 20 March 2020

*Keywords:*
$CO_2$ capture
$CO_2$ corrosion
Carbon steel
Diethanolamine
Piperazine
Electrochemical model

ABSTRACT

A mechanistic model is developed to investigate the influence of an activator on the corrosion rate of carbon steel in the absorption processes of carbon dioxide ($CO_2$). Piperazine (PZ) is used as the activator in diethanolamine (DEA) aqueous solutions. The developed model for corrosion takes into consideration the effect of fluid flow, transfer of charge and diffusion of oxidizing agents and operating parameters like temperature, activator concentration, $CO_2$ loading and pH. The study consists of two major models: Vapor–liquid Equilibrium (VLE) model and electrochemical corrosion model. The electrolyte-NRTL equilibrium model was used for determination of concentration of chemical species in the bulk solution. The results of speciation were subsequently used for producing polarization curves and predicting the rate of corrosion occurring at the surface of metal. An increase in concentration of activator, increases the rate of corrosion of carbon steel in mixtures of activated DEA.



## 1. Introduction

Carbon dioxide ($CO_2$) is one of the major greenhouse gases released to the atmosphere. The quantity of $CO_2$ has risen recently due to rapid urbanization and industrialization [1]. Accumulation of greenhouse gases like $CO_2$ in the atmosphere alters the greenhouse effect leading to global warming and climate change [1,2]. This is connected with the inclination of these gases to act as a blanket for heat in the atmosphere resulting in rapid rise in average global temperatures [3].

Efforts have been taken to reduce the release of $CO_2$ emissions globally. Several technologies like pre-combustion, post-combustion $CO_2$ capture and storage (CCS), oxyfuel combustion, $CO_2$ conversion into fuels and chemicals, membranes for $CO_2$ capture have been introduced to capture and store $CO_2$ as an energy source. So far, CCS have been very successful in implementation at industrial level due to its retrofit option and maturity [4]. Corrosion is one of the undeniable problems for CCS because of $CO_2$ capture using amines as solvents. The mature amine for CCS is the monoethanolamine (MEA), which is very corrosive in nature [5]. Corrosion reduces the plant and equipment life along with operational problems. It is a complicated phenomenon in which chemical, electrochemical processes and transport occur interactively and simultaneously. There is a difficulty in controlling problems of corrosion in a manner that is cost-effective as corrosion knowledge in amine-based CCS is inconclusive and limited [6–8].

Piperazine is a good $CO_2$ capture solvent [9]. It is an effective promotor of chemical absorption when used with amines which have lower absorption kinetics. Piperazine has shown good results as a $CO_2$ absorption promoter in solutions like Methyldiethanolamine (MDEA), Aminomethylpropanol (AMP), Monoethanolamine (MEA), and Diethanolamine (DEA) [10,11]. There has been a limited knowledge on the the corrosion of process materials using blended amines with PZ as the $CO_2$ absorption activator. The knowledge of carbon steel corrosion using amine solvents will help in understanding of the mechanism of corrosion and role of PZ both as a promoter and corrosion agent. Moreover, in literature there are only a few data points on the $CO_2$ corrosion for PZ as an activator.

PZ is known for its corrosion resistance, when compared with benchmark MEA [12]. $CO_2$ loaded PZ helps in quick formation of $FeCO_3$ layer, which inhibits corrosion [13]. $FeCO_3$ forms at rich loading of either fresh or degraded PZ solutions [14]. Nainar and Veawab [15] studied corrosion of PZ and MEA blend for $CO_2$ absorption. The results

* Corresponding author.
*E-mail address:* shaukat.mazari@duet.edu.pk (S.A. Mazari).

https://doi.org/10.1016/j.cjche.2020.03.006
1004-9541/

showed that MEA/PZ blend had higher corrosiveness than the solutions of MEA alone. The rate of corrosion of carbon steel increased with increase in concentration of PZ, total amine concentration, $CO_2$ loading, temperature and presence of heat stable salts. Zhao *et al.* [16] found that PZ has higher influence on corrosion rate of carbon steel while using MDEA/PZ blend under different conditions. Increase in $CO_2$ loading, temperature, amine concentration increased the carbon steel corrosion. However, blend of AMP and PZ has shown a lower corrosion rate due to faster formation of iron carbonate species [17]. Whereas, another study suggests that AMP/PZ blend inhibited corrosion owing to both neutralization and adsorption effects [18]. We [19] previously studied the effect of PZ activated MDEA aqueous solutions on corrosion of carbon steel. Results showed that at low $CO_2$ loading the carbon steel corrosion rate increases with increasing PZ concentration, whereas at high $CO_2$ loading the rate of corrosion declined with the rise of concentration of PZ.

The blend of PZ/DEA has shown good $CO_2$ capture characteristics. The data of PZ/DEA blend is available for its stability, $CO_2$ kinetics, mass-transfer and solubility of $CO_2$. However, no research has been conducted to examine corrosiveness of PZ/DEA solution. This study provides an understanding of corrosion in an aqueous environment for $CO_2$ capture using activated DEA. Emphasis has been given on model development for determining the rate of corrosion in carbon steel, corrosion behavior and mechanism of PZ as an activator for DEA solutions under process operating conditions.

## 2. Corrosion Experiments

### 2.1. Solutions preparation

The amines used in this work were anhydrous Piperazine crystals with purity 99% purchased from Acros Organics, Belgium. Diethanolamine with 98% purity was purchased from Merck Sdn. Bhd. Malaysia. The $CO_2$ with minimum purity of 99.8% and oxygen free nitrogen were purchased from Sitt Tatt Company Sdn. Bhd., Malaysia. Glass microfiber filter paper GF/C, Whatman, were used throughout this research to ensure all the solid carbonates were collected in the analysis section. Carbonated amine solutions were prepared according to the absorption experimental procedure mentioned in our previous work [11]. The partial pressure of carbon dioxide was changed in values (1–100) kPa, at temperatures 40 to 80 °C, with a total amine concentration of 2.0 $mol \cdot L^{-1}$. In DEA/PZ mixtures, the concentration of piperazine ranged from 0.01 to 0.1 $mol \cdot L^{-1}$.

### 2.2. Working electrode

The working sample is made of a rotating electrode, type (EDI 101562R07N002) and specimen. The specimen is made of two constituents, a carbon steel cylinder inserted into Teflon cylinder (insulated materials). Tests were carried out on carbon steel 1020 with the elemental composition of Carbon, Manganese, Phosphorus, Sulfur, Silicon and Iron in ratios of 0.20, 0.51, 0.031, 0.039, 0.17 and balance respectively. The specimen was supplied and manufactured by Radiometer France. It is given the shape of a cylinder and incorporated tight into Teflon. The surface area of the cylinder base was 0.196 $cm^2$ which was made as a disc. The specimen was attached into a rotating electrode which was linked to the radiometer. Carbon steel was selected based on its use in regenerator shell, lean amine cooler tubes, the absorber, and reflux drum. The specimens were grinded with 600 grit silicon carbide papers.

### 2.3. Materials and method

The experiments were conducted in a static corrosion-cell by using electrochemical method for the analysis of corrosion. The experimental apparatus and procedure details are provided by our previous work [19]. Experimental setup is displayed in Fig. 1, which contains the following constituents: corrosion cell, potentiostat/galvanostat PGP201 model and a radiometer FCTV101. The cell includes a 250-ml flask, a platinum wire counter electrode (known as auxiliary electrode), a calomel saturated electrode (known as reference electrode), a vent and purge tube, and a working electrode assembly for specimen mounting. The rest of devices used for corrosion test are like what have been used for the absorption experiment set-up. When a constant pH is reached (amine solution is saturated with $CO_2$), potentiodynamic technique is used manage the tests of corrosion. 600 grit silicon carbide paper was used for polishing the steel operating electrode surface (sample) before every experiment (run) of polarization, and it was then mounted on the holder of sample (working rotating electrode) and was submerged into the solution of electrolyte (corrosion cell containing carbonated solution of amine). The working electrode was exposed to a continuous speed of rotation of 600 $r \cdot min^{-1}$ *via* a radiometer

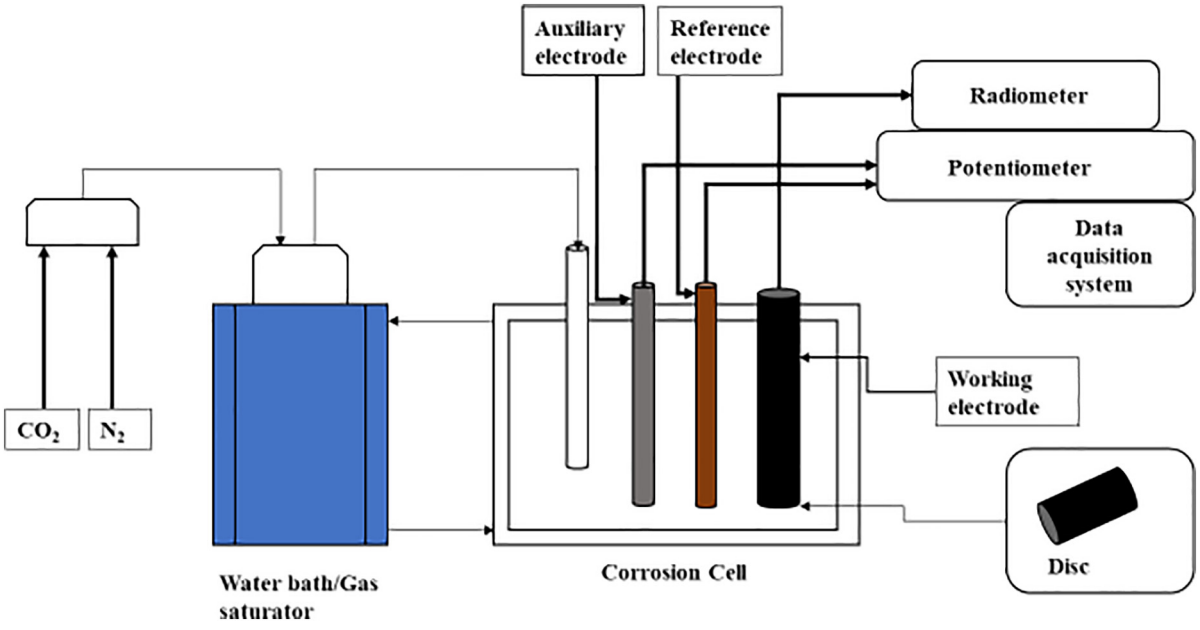


**Fig. 1.** Experimental set up for corrosion experiments [20].

FCTV101 unit of speed control. Platinum wire was used as counter electrode. Potential scanning was affected using a radiometer PGP201 galvanostat/potentiostat linked to a PC for control and data treatment and attainment. The corrosion cell is maintained at the specified temperature, and $CO_2$ partial pressure. The saturated gas was passed into the cell to ensure that the carbonated solution and the $CO_2$ are in equilibrium.

### 2.4. Polarization experiments

The solution of amine was mixed with the coupon holder and vessel of corrosion (with attached weighted cleaned coupons) was soaked in the liquid before lid sealing. At the time of each run, a mixture of gas of $N_2$ and $CO_2$ could enter the cell for reaction until equilibrium of gas–liquid was achieved. Potentio-dynamic technique was applied to perform the experiments of corrosion. The sweep technique of potentio-dynamic was applied to examine the mechanism of corrosion. The sweeps were performed with a scan rate 1.8 $mV \cdot s^{-1}$.

The potential of corrosion ($E_{corr}$) and current density of corrosion ($i_{corr}$) were determined from the intersection of cathodic and anodic curves. EC-Lab software V10.12, 2011 was used to get the Tafel slopes of the curves of polarization. The calculation of the rate of corrosion (CR) can be carried out using Eq. (1):

$$CR = \frac{3.30 \times 10^{-3} \times i_{corr}\, M}{\rho} \tag{1}$$

Where CR in $mm \cdot a^{-1}$, $i_{corr}$ is current density of corrosion ($\mu A \cdot cm^{-2}$); $M$ is the specimen molar weight ($g \cdot mol^{-1}$), and $\rho$ is the specimen density ($g \cdot m^{-3}$).

## 3. Modeling and Speciation Methodology

### 3.1. Model of vapor–liquid equilibrium

The phase equilibrium controls the molecular species distribution between gas phase and the liquid phase and shown by Henry's law (2):

R1: $CO_2$ phase change: $CO_2(g) \overset{K_1}{\rightleftharpoons} CO_2(aq)$

$$H_{CO_2} = \frac{P_{CO_2}}{x_{CO_2}} \tag{2}$$

Where $HCO_2$ is the of Henry's constant of $CO_2$ in the solution of amine; $PCO_2$ is the partial pressure of $CO_2$ in the gas phase at the equilibrium; $xCO_2$ is the liquid phase mole fraction of $CO_2$.

Reactions at equilibrium are the decisive factor of speciation in the liquid bulk. Generally, those are dissociation chemical reactions. The mechanism of reactions for blends including aqueous carbonated PZ + DEA is reported by Bishnoi and Austgen [21,22] as under:

R2: Water Dissociation: $2H_2O \overset{K_2}{\rightleftharpoons} OH^- + H_3O^+$

R3: Dissociation of $CO_2$: $CO_2 + 2H_2O \overset{K_3}{\rightleftharpoons} HCO_3^- + H_3O^+$

R4: Dissociation of bicarbonate ions: $HCO_3^- + H_2O \overset{K_4}{\rightleftharpoons} CO_3^{2-} + H_3O^+$

R5: Dissociation of protonated piperazine: $PZH^+ + H_2O \overset{K_5}{\rightleftharpoons} PZ + H_3O^+$

R6: Formation of piperazine carbamate: $PZ + CO_2 + H_2O \overset{K_6}{\rightleftharpoons} PZCOO^- + H_3O^+$

R7: Dissociation of zwitterion (protonated carbamate): $H^+PZCOO^- + H_2O \overset{K_7}{\rightleftharpoons} PZCOO^- + H_3O^+$.

R8: Dissociation of piperazine carbamate: $PZCOO^- + CO_2 + H_2O \overset{K_8}{\rightleftharpoons} PZ(COO^-)_2 + H_3O^+$

DEA can react directly with $CO_2$ t form carbonate based on the following set of reactions reported by Austgen [22]:

R9: Dissociation of protonated DEA: $DEAH^+ + H_2O \overset{K_9}{\rightleftharpoons} DEA + H_3O^+$

R10: DEA carbamate reversion to bicarbonate and DEA:

$$DEACOO^- + H_2O \overset{K_{10}}{\rightleftharpoons} DEA + HCO_3^-$$

Where $K_i$ is the equilibrium constant for reversible reactions at equilibrium and their values have been extracted from the available open domain literature based on mole fraction as shown in Supplementary Table 1 (ST1). Activity coefficients ($\gamma_i$) and mole fractions ($x_i$) of chemical species have been used for equilibrium constants for the reactions as shown in Eqs. (3) through (11):

$$K_1 = \frac{\left(\gamma_{H_3O^+} x_{H_3O^+}\right)\left(\gamma_{OH^-} x_{OH^-}\right)}{\left(\gamma_{H_2O} x_{H_2O}\right)^2} \tag{3}$$

$$K_2 = \frac{\left(\gamma_{HCO_3^-} x_{HCO_3^-}\right)\left(\gamma_{H_3O^+} x_{H_3O^+}\right)}{\left(\gamma_{CO_2} x_{CO_2}\right)\left(\gamma_{H_2O} x_{H_2O}\right)^2} \tag{4}$$

$$K_3 = \frac{\left(\gamma_{CO_3^{2-}} x_{CO_3^{2-}}\right)\left(\gamma_{H_3O^+} x_{H_3O^+}\right)}{\left(\gamma_{HCO_3^-} x_{HCO_3^-}\right)\left(\gamma_{H_2O} x_{H_2O}\right)} \tag{5}$$

$$K_4 = \frac{\left(\gamma_{PZ} x_{PZ}\right)\left(\gamma_{H_3O^+} x_{H_3O^+}\right)}{\left(\gamma_{PZH^+} x_{PZH^+}\right)\left(\gamma_{H_2O} x_{H_2O}\right)} \tag{6}$$

$$K_5 = \frac{\left(\gamma_{PZCOO^-} x_{PZCOO^-}\right)\left(\gamma_{H_3O^+} x_{H_3O^+}\right)}{\left(\gamma_{PZ} x_{PZ}\right)\left(\gamma_{CO_2} x_{CO_2}\right)\left(\gamma_{H_2O} x_{H_2O}\right)} \tag{7}$$

$$K_6 = \frac{\left(\gamma_{PZCOO^-} x_{PZCOO^-}\right)\left(\gamma_{H_3O^+} x_{H_3O^+}\right)}{\left(\gamma_{H^+PZCOO^-} x_{H^+PZCOO^-}\right)\left(\gamma_{H_2O} x_{H_2O}\right)} \tag{8}$$

$$K_7 = \frac{\left(\gamma_{PZ(COO^-)_2} x_{PZ(COO^-)_2}\right)\left(\gamma_{H_3O^+} x_{H_3O^+}\right)}{\left(\gamma_{PZCOO^-} x_{PZCOO^-}\right)\left(\gamma_{CO_2} x_{CO_2}\right)\left(\gamma_{H_2O} x_{H_2O}\right)} \tag{9}$$

$$K_8 = \frac{\left(\gamma_{DEA} x_{DEA}\right)\left(\gamma_{H_3O^+} x_{H_3O^+}\right)}{\left(\gamma_{DEAH^+} x_{DEAH^+}\right)\left(\gamma_{H_2O} x_{H_2O}\right)} \tag{10}$$

$$K_9 = \frac{\left(\gamma_{DEA} x_{DEA}\right)\left(\gamma_{HCO_3^-} x_{HCO_3^-}\right)}{\left(\gamma_{DEACOO^-} x_{DEACOO^-}\right)\left(\gamma_{H_2O} x_{H_2O}\right)} \tag{11}$$

The concentration calculation of chemical species in the bulk solution needs more equations as shown in Eq. (12) through Eq. (15):

Balance based on electro neutrality:

$$DEAH^+ + PZH^+ + H_3O^+ = HCO_3^- + OH^- + 2\,CO_3^{2-} + PZCOO^- + 2PZ(COO^-)_2 \tag{12}$$

Mole balance for PZ:

$$PZ + PZH^+ + PZCOO^- + H^+PZCOO^- + PZ(COO^-)_2 = PZ_{Total} \tag{13}$$

Mole balance for DEA:

$$DEA + DEAH^+ + DEACOO^- = DEA_{Total} \tag{14}$$

Total mole fraction:

$$\sum_{i=1}^{i=N} x_i = 1.0 \tag{15}$$

Mole balance for $CO_2$:

$$\begin{aligned} &CO_2 + HCO_3^- + CO_3^{2-} + PZCOO^- + H^+PZCOO^- + PZ(COO^-)_2 \\ &\quad + +DEACOO^- \\ &\quad = \alpha_{CO_2}[\text{total Amine}]_{alk} \end{aligned} \tag{16}$$

At equilibrium the fugacity of components in vapor and liquid phase is assumed to be equal. Eq. (17) is related to the $CO_2$ molecules distribution between the vapor and liquid phase at equilibrium, whereas Eq. (18) is related to the species of solvent (water, DEA, and PZ) as per activity coefficient approach [28].

$$\varnothing_{CO_2}^{v} y_{CO_2} P = \gamma_{CO_2}^{*} x_{CO_2} H_{CO_2}^{\infty} \exp\left(\frac{\upsilon_{CO_2}^{\infty}\left(P - P_W^{\circ}\right)}{RT}\right) \tag{17}$$

$$\varnothing_i^{v} y_i P = \gamma_i x_i P_i^{\circ} \varnothing_i^{\circ} \exp\left(\frac{\upsilon_i\left(P - P_i^{\circ}\right)}{RT}\right) \tag{18}$$

Where $y_i$ and $x_i$ are vapor and liquid phase concentrations respectively for species; $\upsilon_{CO_2}^{\infty}$ is the partial molar volume of $CO_2$ that is diluted infinitely in water, and $\upsilon_i$ is the partial molar volume of solvent of pure liquid determined by Rackett equation of state [29]. The fugacity coefficients of vapor phase in Eqs. (17) and (18) are calculated by the use of the Soave–Redlich-Kwong (SRK) equation of state [30] and the e-NRTL model was used to calculate the liquid phase activity coefficients. The excess Gibbs energy was also calculated using e-NRTL through Eq. (19) [22,31–33]:

$$\frac{G^{ex}}{RT} = \frac{G^{ex,PDH}}{RT} + \frac{G^{ex,Born}}{RT} + \frac{G^{ex,lc}}{RT} \tag{19}$$

$$\frac{G^{ex,PDH}}{RT} = -\sum_k x_k \left(\frac{1000}{M_s}\right)^{\frac{1}{2}} \left(\frac{4A_\phi I_x}{\rho}\right) \ln\left(1 + \rho I_x^{\frac{1}{2}}\right) \tag{20}$$

Debye–Hückel parameter $A_\phi$ and ionic solvent strength $I_x$ are given by Eqs. (21) and (22), respectively.

$$A_\phi = \frac{1}{3}\left(\frac{2\pi N_A d_s}{1000}\right)^{\frac{1}{2}} \left(\frac{e^2}{DkT}\right)^{\frac{3}{2}} \tag{21}$$

$$I_x = \frac{1}{2}\sum_i x_i Z_i^2 \tag{22}$$

The term of Born correction for the excess Gibbs energy is shown by Eq. (23):

$$\frac{G^{ex,Born}}{RT} = \left(\frac{e^2}{2kT}\right)\left(\frac{1}{D} - \frac{1}{D_w}\right)\left(\sum_i \frac{x_i z_i^2}{r_i}\right) \times 10^{-2} \tag{23}$$

The calculation of the mixed dielectric solvent constant, $D_s$, is given by an average of simple mass fraction [32]. The dielectric constants of all components of solvent system are given in Supplementary (ST2).

Eqs. (24) and (25) have been used to calculate the dielectric constants for $H_2O$, DEA, and PZ.

$$D = a_1 + b_1/T\left[\frac{1}{T} - \frac{1}{T^{ref}}\right] \tag{24}$$

Where $T^{ref}$ is the temperature of reference (273.15 K). For mixture of solvents, the calculation of the dielectric constant is given according to the Eq. (25):

$$D_m = \sum_i w_{mi}^{sf} D_i \tag{25}$$

Where $w_{m_i}^{sf}$ is the solute free, solvent fraction.

The expression of the local electrolyte NRTL for the interactions is given in Eq. (26):

$$\begin{aligned} \frac{G^{ex,lc}}{RT} &= \sum_m X_m \frac{\sum_j X_j G_{jm} \tau_{jm}}{\sum_k X_k G_{km}} \\ &\quad + \sum_c X_c \sum_{a'} \left(\frac{X_{a'}}{\sum_{a''} X_{a''}}\right) \frac{\sum_j X_j G_{jc,a'c}\, \tau_{jc,a'c}}{\sum_k X_k G_{kc,a'c}} \\ &\quad + \sum_a X_a \sum_{c'} \left(\frac{X_{c'}}{\sum_{c''} X_{c''}}\right) \left(\frac{\sum_j X_j G_{ja,c'a}\, \tau_{ja,c'a}}{\sum_k X_k G_{ka,c'a}}\right) \end{aligned} \tag{26}$$

Where $j$ and $k$ are any species, and other quantity terms are presented in Eq. (27) through (30).

$$G_{jc,a'c} = \exp\left(-\alpha_{jc,a'c}\, \tau_{jc,a'c}\right) \tag{27}$$

$$G_{ja,c'a} = \exp\left(-\alpha_{ja,c'a}\, \tau_{ja,c'a}\right) \tag{28}$$

$$\tau_{cm} = -\frac{\ln G_{cm}}{\alpha_{cm}} \tag{29}$$

**Table 1**
Literature datasets for development of model and their average absolute deviation (%) of predicted and measured values for $CO_2$ solubility for solutions of DEA and activated DEA systems

| Reference | DEA /mol·L$^{-1}$ | PZ /mol·L$^{-1}$ | $T$ /K | $PCO_2$ /kPa | No. data point | AAD/% |
|---|---|---|---|---|---|---|
| [23] | 6.825 | | 298.13–348.07 | 2.46–4662.7 | 25 | 12.47 |
| [24] | 2 | | 303–323 | 0.09–104.727 | 24 | 6.85 |
| | 4 | | | 0.095–102.12 | 21 | 14.57 |
| [25] | 4.2 | | 373.2 | 93–3742 | 6 | 5.9 |
| [26] | 0.525 | | 273.15–413.2 | 0.6895–6895 | 308 | 13.62 |
| | 2.47 | | | | | |
| | 5.22 | | | | | |
| | 9.41 | | | | | |
| | 16.7 | | | | | |
| | 33 | | | | | |
| [11] | 2 | 0 | 313–353 | 0.01–100 | 60 | 14.59 |
| | 1.98 | 0.01 | | | | |
| | 1.9 | 0.05 | | | | |
| | 1.8 | 0.1 | | | | |
| [27] | 3.2–0.8 | 0.02–0.8 | 313–353 | 10.13–20.265 | 44 | 0.68 |

**Table 2**
Data for development of model and their average absolute deviation (%) of predicted and measured values of pH for solutions of DEA and activated DEA systems

| Reference | DEA/mol·L$^{-1}$ | PZ/mol·L$^{-1}$ | $T$/°C | $PCO_2$/kPa | No. data point | AAD/% |
|---|---|---|---|---|---|---|
| [11] | 2.0 | 0 | 313–353 | 0.01–100 | 48 | 6.18 |
| | 1.98 | 0.01 | | | | |
| | 1.9 | 0.05 | | | | |
| | 1.8 | 0.1 | | | | |

$$\tau_{am} = -\frac{\ln G_{am}}{\alpha_{am}} \tag{30}$$

Where $X_j$ is the effective mole fraction of liquid-phase, $X_j = x_j.C_j$ ($C_j = Z_j$ for ions and 1 given for molecules). $\alpha_{ij}$ is the non-randomness parameter of e-NRTL; $\tau_{ij}$ is the binary parameter of energy interaction. Both $\alpha$ and $\tau$ are regarded as parameters that are adjustable of the expression of the electrolyte NRTL. The activity coefficients of any species (molecular, ionic, solvent, or solute) were calculated from expressing the partial derivative of the excess Gibbs energy Eq. (31):

$$\ln\gamma_i = \frac{1}{RT}\left[\frac{\partial(n_t G^{ex})}{\partial n_i}\right]_{T,P,n_{j\neq i}} \quad i,j = m,c,a \tag{31}$$

There are some binary parameters and pure components that are involved in equilibrium model of vapor liquid equilibrium developed above as: Brelvi-O'Connell parameter, critical constants, compressibility factor, and acentric factor. Moreover, to solve the Antoine equation the constants for vapor pressure of different molecular species are obtained from literature and shown in Supplementary ST3 and ST4.

The parameter of non-randomness was proposed by the study of Chen & Evans [31] and Mock *et al.* [32]. Parameters of binary interaction for ion pair–ion pair, molecule–molecule, and molecule–ion pair are expressed as a function of temperature as illustrated by Eq. (32) through (33).

$$\tau_{m,ca} = A_{ca,m} + \frac{B_{m,ca}}{T} \tag{32}$$

$$\tau_{ca,m} = A_{ca,m} + \frac{B_{ca,m}}{T} \tag{33}$$

These binary parameters are categorized into three groups; molecule–molecule pair, molecule–ion pair, and ion pair–ion pair interactions from the work of Austgen *et al.* [22] and Pitzer [34] shown in ST5.

The bulk concentration of carbonated species in the solution of aqueous concentrations of DEA-PZ were calculated using MATLAB program. Concentrations of all species were not known and defined as dependent variables, except the $CO_2$ concentration, whose calculation was given from the Eq. (2). For DEA-PZ aqueous solutions, it is necessary to solve fourteen equations with fourteen variables. In this case, Eqs. (3) to (16) can be decreased to a single polynomial equation of eight order in relation to concentration of hydronium ion [$H_3O^+$], equilibrium constants and initial amine concentration. The values of [$H_3O^+$] relate to the pH of solution at equilibrium, whereas more possible roots for each partial pressure of $CO_2$ may be available. One value of only [$H_3O^+$] is valid and supposed to be in between $10^{-6}$ mol·L$^{-1}$ and $10^{-12}$ mol·L$^{-1}$, which corresponds to the values of pH of a carbonated solution of amine, and commercial application value is normally 6–12. Non-linear equations were simultaneously solved through iteration process. The solution resulted in finding the concentration of the chemical species in the bulk solution and activity coefficients. The loading of $CO_2$ in amine systems for absorption is determined by using Eq. (16).

### 3.2. Electrochemical corrosion model

The electrochemical reactions happening simultaneously at the interface of metal-solution are regarded as metal oxidation (iron dissolution) and reduction oxidizing agents. One oxidation reaction (Fe) and five reduction reactions are considered to take place in the DEA-PZ system:

Iron Oxidation: $Fe \rightleftharpoons Fe^{2+} + 2e^-$
Hydronium ion reduction: $2H_3O^+ + 2e^- \rightleftharpoons 2H_2O + H_2$
Bicarbonate ion Reduction: $2HCO_3^- + 2e^- \rightleftharpoons 2CO_3^{2-} + H_2$
Reduction of water: $2H_2O + 2e^- \rightleftharpoons 2OH^- + H_2$
Reduction of $PZH^+$ ion: $2PZH^+ + 2e^- \rightleftharpoons 2PZ + H_2$
Reduction of $DEAH^+$ ion: $2DEAH^+ + 2e^- \rightleftharpoons 2DEA + H_2$

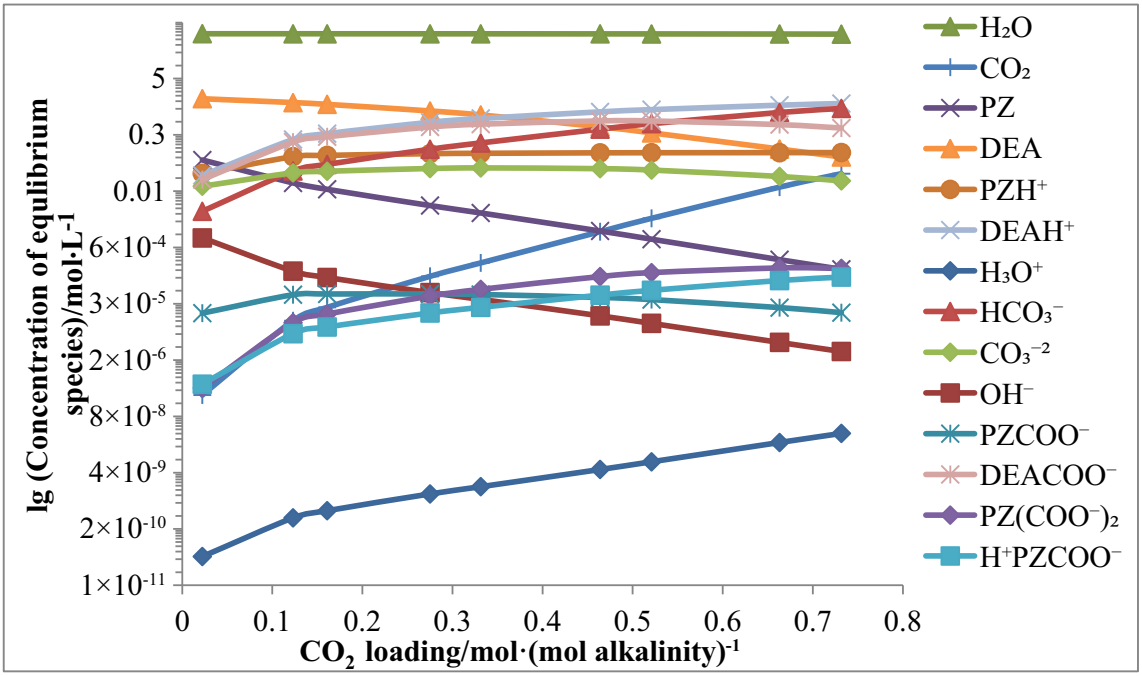


**Fig. 2.** Predicted concentration of species in 1.8 mol·L$^{-1}$ DEA + 0.1 mol·L$^{-1}$ PZ system at 40 °C.

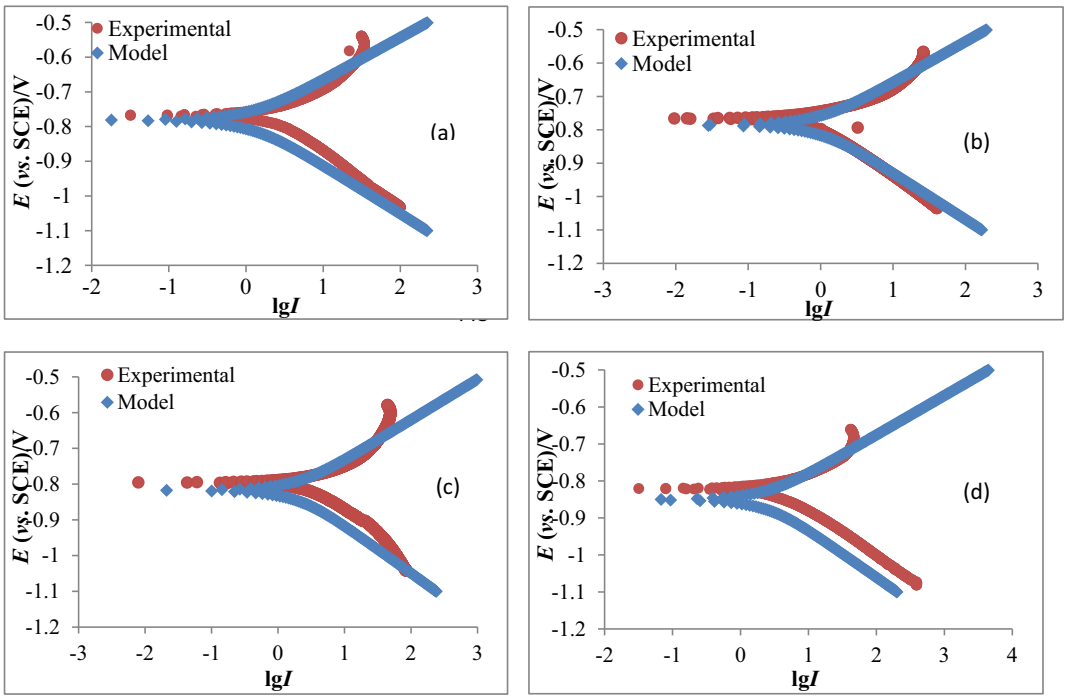


**Fig. 3.** Comparison of experimental and predicted polarization curves of carbon steel in (a) 1.98 mol·L$^{-1}$ DEA + 0.01 mol·L$^{-1}$ PZ; $PCO_2$ = 95.4 kPa at 40 °C. (b)1.9 mol·L$^{-1}$ DEA + 0.05 mol·L$^{-1}$ PZ; $PCO_2$ = 47.72 kPa at 40 °C. (c) 1.98 mol·L$^{-1}$ DEA + 0.01 mol·L$^{-1}$ PZ; $PCO_2$ = 83.07 kPa at 40 °C. (d) 1.8 mol·L$^{-1}$ DEA + 0.1 mol·L$^{-1}$ PZ; $PCO_2$ = 56.14 kPa at 80 °C.

Carbonic acid is regarded to be "weak acid" due to its dissociation that is partial in water to generate $H^+$ ions and $HCO_3^-$ ion.

$$2H_2CO_3 + 2e^- \rightleftharpoons 2HCO_3^- + H_2$$

Since carbonated solutions of activated DEA system are alkaline and the contribution of the reduction reaction of $H_2CO_3$ is neglected due to very low concentration in the solution in comparison with other species, the dissolution of iron was regarded to be under control of activation (charge transfer) due to the unlimited supply of Fe. In this case, the relation between potential ($E$) and the current density ($i$) was presented as in Eq. (34) and (35):

$$i_{Fe/Fe^{2+}} = i_{o,Fe/Fe^{2+}} \times 10^{\left(\frac{E-E_{rev}}{\beta_a}\right)} \quad (34)$$

$$\beta_a = \frac{2.303\,RT}{n\,\alpha_a F} \quad (35)$$

The oxidization agents for the reduction reactions involving in the process of corrosion are $H_3O^+$, $HCO_3^-$, $H_2O$, $PZH^+$, and $DEAH^+$. The total rate of reduction will be as in Eq. (36):

$$\sum i_{reduction} = i_{H_3O^+/H_2} + i_{HCO_3^-/CO_3^{2-}} + i_{H_2O/OH^-} + i_{PZH^+/PZ} + i_{DEAH^+/DEA} \quad (36)$$

For reduction reactions on the metal surface, the cathodic reactions are considered to be under mixed control which take into account the effect of mass transfer and charge transfer. Supposed that the rate of $H_2O$ is governed by charge transfer control because the water molecules are found in unlimited quantities at the metal surface. For ($k$) reduction

**Table 3**
Comparison of the model results for rate of corrosion with experimental data for diethanolamine (2 mol·L$^{-1}$ DEA)

| $T$ /°C | $PCO_2$ /kPa | Experimental | | Model | | $\delta^a$ | $\delta^b$ |
|---|---|---|---|---|---|---|---|
| | | $E_{corr}$ (*vs.* SCE)/V | CR /mm·a$^{-1}$ | $E_{corr}$ (*vs.* SCE)/V | CR /mm·a$^{-1}$ | | |
| 40 | 0.96 | −0.8100 | 0.212 | −0.78468 | 0.2023 | 3.13 | 4.59 |
| | 9.59 | −0.7837 | 0.795 | −0.79341 | 0.6289 | 1.23 | 20.90 |
| | 47.89 | −0.7687 | 1.033 | −0.79136 | 1.1745 | 2.94 | 13.70 |
| | 95.61 | −0.7655 | 1.314 | −0.7868 | 1.4608 | 2.78 | 11.17 |
| 60 | 0.83 | −0.8088 | 0.483 | −0.79518 | 0.2177 | 1.69 | 54.93 |
| | 8.31 | −0.8063 | 1.499 | −0.80296 | 0.8377 | 0.42 | 44.11 |
| | 41.62 | −0.7993 | 1.349 | −0.80343 | 1.7887 | 0.51 | 32.60 |
| | 83.41 | −0.7939 | 2.221 | −0.80098 | 2.3516 | 0.89 | 5.88 |
| 80 | 0.556 | −0.8865 | 0.188 | −0.79537 | 0.1720 | 10.28 | 8.52 |
| | 5.54 | −0.8485 | 1.106 | −0.80951 | 0.7573 | 4.60 | 31.53 |
| | 41.45 | −0.7951 | 4.469 | −0.8126 | 2.3579 | 2.19 | 47.24 |
| | 55.64 | −0.7917 | 4.637 | −0.81225 | 2.7260 | 2.59 | 41.21 |

Note : $\delta^a = \frac{|E_{corr(Cal.)} - E_{corr(Exp.)}|}{E_{corr(Exp.)}} \times 100, \delta_{AAD} = 2.77\%$

$\delta^b = \frac{|CR_{(Cal.)} - CR_{(Exp.)}|}{CR_{(Exp.)}} \times 100, \delta_{AAD} = 26.36\%$

**Table 4**
Comparison of the model results for corrosion rate with experimental data (for 1.98 mol·L$^{-1}$ DEA + 0.01 mol·L$^{-1}$ PZ)

| $T$ /°C | $PCO_2$ /kPa | Experimental | | Model | | $\delta^a$ | $\delta^b$ |
|---|---|---|---|---|---|---|---|
| | | $E_{corr}$ (*vs.* SCE)/V | CR /mm·a$^{-1}$ | $E_{corr}$ (*vs.* SCE)/V | CR /mm·a$^{-1}$ | | |
| 40 | 0.96 | −0.8154 | 0.229 | −0.7850 | 0.2041 | 3.72 | 10.87 |
| | 9.59 | −0.7760 | 0.738 | −0.7936 | 0.6315 | 2.27 | 14.43 |
| | 47.89 | −0.7887 | 0.764 | −0.7914 | 1.1763 | 0.35 | 53.97 |
| | 95.44 | −0.7678 | 1.287 | −0.7868 | 1.4603 | 2.48 | 13.47 |
| 60 | 0.83 | −0.82481 | 0.56 | −0.7959 | 0.2207 | 3.50 | 60.58 |
| | 8.32 | −0.81693 | 0.87 | −0.8033 | 0.8433 | 1.66 | 3.07 |
| | 41.54 | −0.80293 | 1.63 | −0.8036 | 1.7911 | 0.09 | 9.89 |
| | 83.07 | −0.79551 | 2.43 | −0.8011 | 2.3499 | 0.71 | 3.29 |
| 80 | 0.55 | −0.82810 | 0.35 | −0.797 | 0.1754 | 3.76 | – |
| | 5.55 | −0.81680 | 1.363 | −0.8103 | 0.7669 | 0.79 | 43.73 |
| | 27.91 | −0.81587 | 3.071 | −0.8131 | 1.9313 | 0.33 | 37.11 |
| | 55.81 | −0.81725 | 2.995 | −0.8126 | 2.7383 | 0.57 | 8.57 |

Note : $\delta^a = \frac{|E_{corr(Cal.)} - E_{corr(Exp.)}|}{E_{corr(Exp.)}} \times 100, \delta_{AAD} = 1.69\%$

$\delta^b = \frac{|CR_{(Cal.)} - CR_{(Exp.)}|}{CR_{(Exp.)}} \times 100, \delta_{AAD} = 25.74\%$

**Table 5**
Comparison of the model results for corrosion rate with experimental data (for 1.9 mol·L$^{-1}$ DEA + 0.05 mol·L$^{-1}$ PZ)

| $T$ /°C | $PCO_2$ /kPa | Experimental | | Model | | $\delta^a$ | $\delta^b$ |
|---|---|---|---|---|---|---|---|
| | | $E_{corr}$ (*vs.* SCE)/V | CR/mm·a$^{-1}$ | $E_{corr}$ (*vs.* SCE)/V | CR /mm·a$^{-1}$ | | |
| 40 | 0.96 | −0.8168 | 0.241 | −0.7866 | 0.2124 | 3.70 | 11.88 |
| | 9.59 | −0.7708 | 0.651 | −0.7945 | 0.6425 | 3.08 | 1.30 |
| | 47.72 | −0.7662 | 0.946 | −0.7917 | 1.1823 | 3.34 | 24.98 |
| | 95.78 | −0.7699 | 1.26 | −0.7867 | 1.4637 | 2.20 | 16.17 |
| 60 | 0.83 | −0.7979 | 0.424 | −0.7989 | 0.2353 | 0.14 | 44.51 |
| | 8.31 | −0.8006 | 0.952 | −0.8050 | 0.8630 | 0.56 | 9.35 |
| | 41.62 | −0.7785 | 1.989 | −0.8046 | 1.8084 | 3.35 | 9.08 |
| | 83.41 | −0.7593 | 1.718 | −0.8017 | 2.3620 | 5.60 | 37.48 |
| 80 | 0.56 | −0.7960 | 0.278 | −0.8037 | 0.1967 | 0.97 | 29.26 |
| | 5.58 | −0.7959 | 0.893 | −0.8136 | 0.8060 | 2.23 | 9.74 |
| | 27.82 | −0.7916 | 2.423 | −0.8151 | 1.9676 | 2.97 | 18.80 |
| | 55.14 | −0.7802 | 2.7 | −0.8141 | 2.7565 | 4.35 | 2.09 |

Note : $\delta^a = \frac{|E_{corr(Cal.)} - E_{corr(Exp.)}|}{E_{corr(Exp.)}} \times 100, \delta_{AAD} = 2.71\%$

$\delta^b = \frac{|CR_{(Cal.)} - CR_{(Exp.)}|}{CR_{(Exp.)}} \times 100, \delta_{AAD} = 17.89\%$

**Table 6**
Comparison of the model results of corrosion rate with experimental data (for 1.8 mol·L$^{-1}$ DEA + 0.1 mol·L$^{-1}$ PZ)

| $T$/°C | $PCO_2$ /kPa | Experimental | | Model | | $\delta^a$ | $\delta^b$ |
|---|---|---|---|---|---|---|---|
| | | $E_{corr}$(*vs.* SCE)/V | CR/mm·a$^{-1}$ | $E_{corr}$ (*vs.* SCE)/V | CR/mm·a$^{-1}$ | | |
| 40 | 0.96 | −0.7801 | 0.30 | −0.7887 | 0.2235 | 1.10 | 645.04 |
| | 9.59 | −0.7919 | 0.47 | −0.7957 | 0.6572 | 0.48 | 39.84 |
| | 47.72 | −0.7569 | 1.29 | −0.7921 | 1.1915 | 4.66 | 7.63 |
| | 95.61 | −0.7676 | 1.21 | −0.7868 | 1.4646 | 2.50 | 21.04 |
| 60 | 0.83 | −0.7638 | 0.54 | −0.8029 | 0.2549 | 5.11 | 52.79 |
| | 8.36 | −0.7969 | 0.85 | −0.8072 | 0.8928 | 1.29 | 5.03 |
| | 41.28 | −0.8032 | 1.95 | −0.8058 | 1.8238 | 0.33 | 6.47 |
| | 83.58 | −0.7897 | 1.47 | −0.8025 | 2.3747 | 1.62 | 61.54 |
| 80 | 0.56 | −0.7977 | 0.70 | −0.8113 | 0.2221 | 1.71 | 68.27 |
| | 5.56 | −0.7977 | 0.504 | −0.8179 | 0.8535 | 2.53 | 69.35 |
| | 27.74 | −0.8190 | 0.96 | −0.8176 | 2.0172 | 0.18 | 110.12 |
| | 56.15 | −0.8206 | 2.97 | −0.8159 | 2.8251 | 0.56 | 4.88 |

Note : $\delta^a = \frac{|E_{corr(Cal.)} - E_{corr(Exp.)}|}{E_{corr(Exp.)}} \times 100, \delta_{AAD} = 1.84\%$

$\delta^b = \frac{|CR_{(Cal.)} - CR_{(Exp.)}|}{CR_{(Exp.)}} \times 100, \delta_{AAD} = 39.37\%$

reaction system, the rate equation is shown in Eq. (37):

$$i_k = i_{o(k)} \times \left\{ \frac{[k]_s}{[k]_b} \times \exp\left( -\frac{n\,\alpha_c F}{RT}(E - E_{rev}) \right) \right\} \tag{37}$$

Where $i_k$ is of reduction reaction current density ($A \cdot m^{-2}$). $i_o$ is the current density of equilibrium exchange of a reaction ($A \cdot m^{-2}$). $[k]_s$ is the concentration of agent species on surface that are oxidizing ($mol \cdot L^{-1}$). $[k]_b$ is the concentration of the bulk of agent species that are oxidizing ($mol \cdot L^{-1}$). $\alpha_c$ is the factor of cathodic symmetry. $n$ is the number of electrons transferred in the reduction reaction. $F$ is the constant of Faraday ($C \cdot mol^{-1}$), and $E$ is the potential (V *vs.* SCE). The determination of concentration of surface on the electrode can be done from the mass-transport equation as shown in Eq. (38):

$$i_k = k_m F \{ [k]_b - [k]_s \} \tag{38}$$

Where $k_m$ is the mass-transfer coefficient of reduction reaction ($m \cdot s^{-1}$). Eq. (37) substitution into (38) as well as solving for $[k]_s$ produces the final current *versus* voltage equation for reactions of reduction:

$$\frac{1}{i_k} = \frac{1}{i_{act(k)}} + \frac{1}{i_{lim(k)}} \tag{39}$$

Where $i^d_{lim(k)}$ is the diffusion limiting current density in $A \cdot m^{-2}$, and $i_{act(k)}$ is the contribution of charge transfer to the current density without the existence of mass transfer resistance, which is given by Eq. (40):

$$i_{act(k)} = i_{o(k)} \times 10^{\left( -\frac{(E - E_{rev})}{\beta_c} \right)} \tag{40}$$

Where $i_{o(k)}$ is the current density of equilibrium exchange in $A \cdot m^{-2}$, and $\beta_c$ is the cathodic Tafel slope in V/dec. Nernst equation is used to calculate the reversible potential $E_{rev}$ (V) of each reaction as described in Eq. (41):

$$E_{rev} = E^o_T + \frac{RT}{nF} \ln\left( \frac{a_{prod.}}{a_{react.}} \right) \tag{41}$$

Where $E^o_T$ is the standard electrode potential (V *versus* SCE) at any temperature given; $R$ is the universal gas constant ($J \cdot mol^{-1} \cdot K^{-1}$); $T$ is the absolute temperature (K); $n$ is number of electrons contributing in the reaction. $a_{prod.}$ and $a_{react.}$ are the reactant and product activities, respectively; $F$ is the Faraday's constant ($C \cdot mol^{-1}$). The $E^o_T$ was calculated by using Eq. (42):

$$\Delta G^o_T = -n_i F E^o_T \tag{42}$$

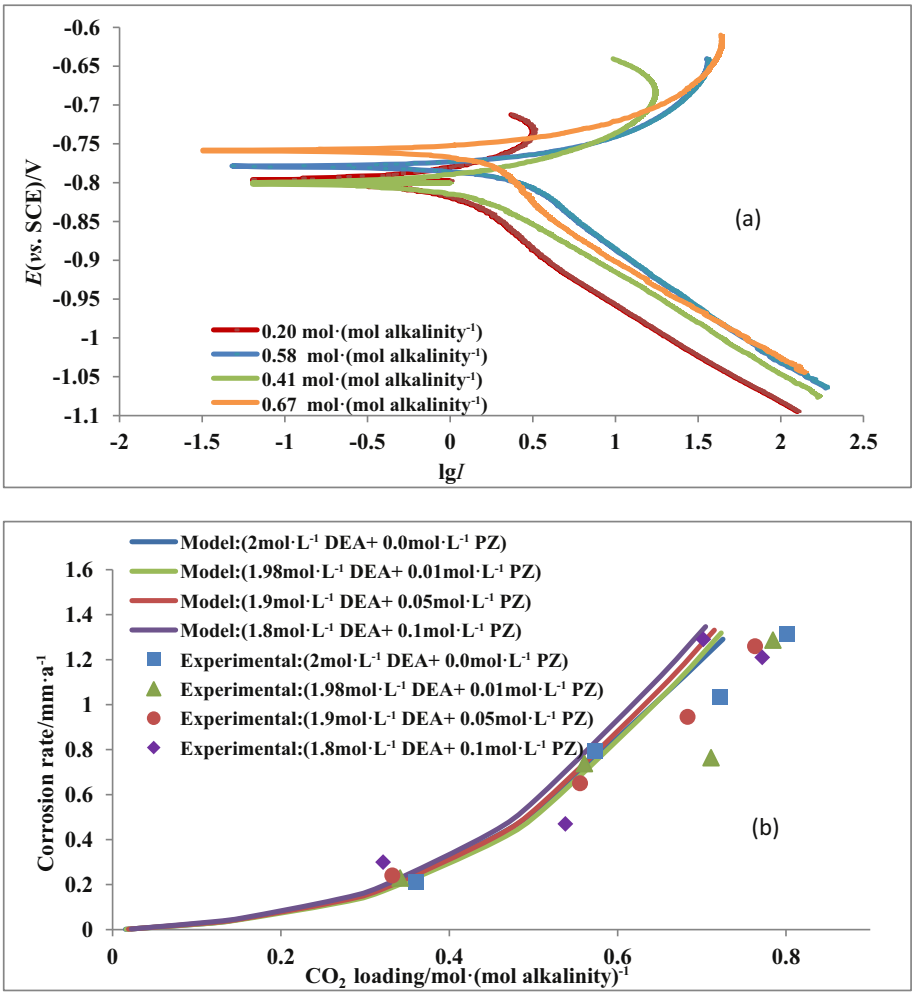


**Fig. 4.** Effect of $CO_2$ loading on (a) carbon steel polarization behavior in solution of DEA-PZ ( 1.9 $mol \cdot L^{-1}$ DEA + 0.05 $mol \cdot L^{-1}$ PZ) at 60 °C and (b) corrosion rate of carbon steel rate in activated aqueous DEA solutions at 40 °C.

Where $\Delta G_T^o$ is the Gibbs free energy of formation any compound at a given temperature, which can be determined using Eq. (43);

$$\Delta G_T^o = T\left[\frac{\Delta G_r^o}{298.15} + \Delta H_r^o\left(\frac{1}{T} - \frac{1}{298.15}\right)\right] \quad (43)$$

Where $\Delta G_r^o$ and $\Delta H_r^o$ are Gibbs energy of reaction ($kJ \cdot mol^{-1}$) at 298.5 K and standard enthalpy of reaction ($kJ \cdot mol^{-1}$) at 298.15 respectively, and $T$ represents the system temperature (K). The values of $\Delta G_r^o$ and $\Delta H_r^o$ are shown in ST6. Whereas the exchange current density is provided by Eq. (44):

$$i_o = i_{o,ref}\left(\frac{C_{ox}}{C_{ox,ref}}\right)^n \exp\left(-\frac{E_a}{R}\left(\frac{1}{T} - \frac{1}{T_{ref}}\right)\right) \quad (44)$$

Where $E_a$ is the activation energy in $kJ \cdot mol^{-1}$, and $i_o^{ref}$ is the exchange current density measured at reference temperature, $T_{ref}$ and reference concentration of oxidizing agent; $C_{ox}$ is the oxidizing agent concentration, and $n$ is the reaction order. Mechanisms and data were found in the open literature related to the reactions which were regarded in the current work only the exchange current density for $PZH^+$ and $DEAH^+$ reduction reaction which were supposed to be the same as of $MDEAH^+$ reduction. The total limiting current density is shown in Eq. (45):

$$i_{\lim(k)} = nFk_m[k]_b \quad (45)$$

Where $k_m$ is the mass transfer coefficient ($s^{-1}$) and is presented into Sherwood ($Sh$) number, for rotating electrode disc; the laminar mass transport equation is considered by Levich [35]:

$$Sh = \frac{k_m d}{D_i} = 0.621\ Re^{0.5}\ Sc^{0.33} \quad (46)$$

Where $d$ is the diameter of rotating disc (m); $D_i$ is a reacting species diffusion coefficient ($m^2 \cdot s^{-1}$); $Re$ and $Sc$ represent Schmidt and Reynolds numbers respectively. The diffusion coefficient is determined by Stokes–Einstein equation for various species as a function of temperature:

$$D = D_{ref} \times \frac{T}{T_{ref}} \times \frac{\mu_{ref}}{\mu} \quad (47)$$

Where $D_{ref}$ is the species diffusion coefficient in water at the reference temperature ($T_{ref}$); $\mu_{ref}$ is the dynamic viscosity of mixed solution of alkanolamine at reference temperature, and $\mu$ is the viscosity of mixed solution of alkanolmines at any temperature ($T$). The values of diffusion coefficient for ionic species are given in ST7, and the diffusion coefficients of the protonated alkanolamine have been considered equal to that of molecular amine [36]. The equation of Weiland can be used for the carbonated systems as given in Eq. (48):

$$\mu_{mix} = \frac{w_1}{w_1} + w_2\mu_{1,\alpha} + \frac{w_2}{w_1} + w_2\mu_{2,\alpha} \quad (48)$$

Where $\mu_{mix}$ is the viscosity of carbonated aqueous activated DEA solutions; $\mu_1$ and $\mu_2$ are the viscosities of the single alkanolamines in water at loading $\alpha$, and $w_i$ is the mass fraction of amine $i$. The viscosity of single alkanolamine (Pa·s) can be calculated from the following equation [37]:

$$\mu_i = \mu_{H_2O} \exp\left[\frac{[(a_iw_1 + b_i)T + (c_iw_1 + d_i)][\alpha(e_iw_1 + f_iT + g_i) + 1]w_1}{T^2}\right] \quad (49)$$

Where $\mu_{H_2O}$ is the water viscosity ($kg \cdot m^{-1} \cdot s^{-1}$) at any temperature $T$; $T$ is the temperature given (K), $\alpha$ is represent $CO_2$ loading (mol $CO_2$·(mol amine)$^{-1}$); $w_1$ stands for amine mass percent, and the constant values in Eq. (49) are provided in ST8. The determination of value of $\mu_{H2O}$ was carried out as a function of temperature as described in Eq. (50) [38]:

$$\mu_{H_2O} = \mu_{H_2O,ref} \times 10^{\left(\frac{1.3277(20-T) - 0.001053(T-20)^2}{T-105}\right)} \quad (50)$$

Where $\mu_{H_2O,\ 20°C}$ is the water viscosity at 20 °C (0.001002 Pa·s).

The electrochemical model was solved using MATLAB software 2017a. Model-required inputs: temperature (K), oxidizing agent species concentration ($mol \cdot L^{-1}$), and the hydrodynamic parameters for rotating disc ($rad \cdot s^{-1}$) and diameter of disc (m). Once input parameters found and selected, the model calculates total and individual anodic and cathodic currents density. The total cathodic curve intersection with the anodic curve to provide with corrosion potential ($E_{corr}$) from Eq. (51). The calculation of current density of corrosion ($i_{corr}$) is done from anodic current equation at $E = E_{corr}$. The carbon steel corrosion rate ($mm \cdot a^{-1}$) was calculated from the corrosion current density value $i_{corr}$ in ($A \cdot m^{-2}$), as described in Eq. (51).

$$i_{Fe/Fe^{2+}} = i_{H_3O^+/H_2} + i_{HCO_3^-/CO_3^{2-}} + i_{H_2O/OH^-} + i_{PZH^+/PZ} + i_{MDEAH^+/MDEA} \quad (51)$$

Tafel method for extrapolation was used for the determination of current density of corrosion, which gives the calculation of rate of the corrosion as shown in Eq. (52):

$$CR = \frac{i_{corr}M_{Fe}}{\rho_{Fe}\,nF} \quad (52)$$

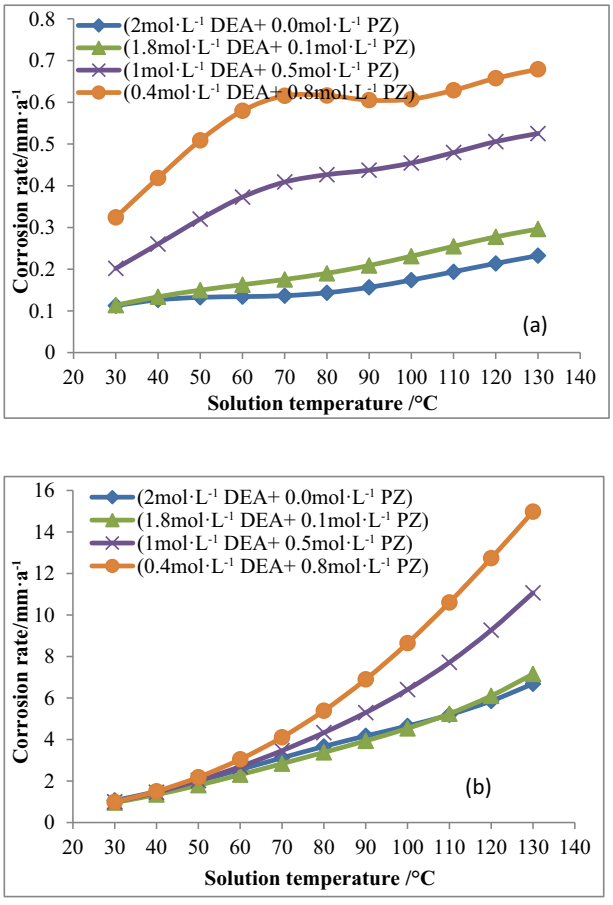


**Fig. 5.** Effect of temperature on rate of corrosion of carbon steel in aqueous solutions of DEA-PZ at (a) low $CO_2$ loading and (b) at high $CO_2$ loading.

Applying Eq. (52) for carbon steel (MW = 55.854 kg·kmol$^{-1}$, ρ = 7800 kg·m$^{-3}$) by having transfer of 2 mol of electrons. Moreover, this equation can be changed to more traditional and convenient sets of units shown as in Eq. (53):

$$CR = 1.155 \times i_{corr} \quad (53)$$

## 4. Results and Discussion

### 4.1. DEA-PZ system speciation in carbonated solutions

To validate the VLE model, experimental data for the loading of $CO_2$ and pH have been taken from literature. The comparison was made under a wide range of operating conditions as shown in Tables 1 and 2. The amounts of $CO_2$ absorbed in a range of solutions are calculated through model and measured through experiments are compared in Table 1. The deviation between measured and calculated values is less than 9.81%. This difference could be caused by the parameters of interaction between molecules and ions, which were regarded as a parameter of default from the work of Austgen [22]. This can be attributable to the fact that the Henry's constants were applied in this study, which were taken from the study of Austgen [22]. Low partial pressure data of $CO_2$ show relatively large errors, which may be because of limitations in the experimental technique/setup used for VLE.

The VLE model was used for the determination of concentration of all chemical species in DEA-PZ solution bulk under a wide range of operating conditions. The data were obtained under operating parameters like $CO_2$ loading of solution, temperature of solution, and concentration of PZ.

Low PZ species have been found compared to DEA due to low concentration of piperazine in DEA solutions to that of DEA. Fig. 2 reflects the predicted carbonated aqueous solution speciation of 1.8 mol·L$^{-1}$ DEA + 0.1 mol·L$^{-1}$ PZ at 40 °C. Both PZ and DEA form carbamate species. PZ have a faster reaction than DEA with $CO_2$. No major variations in behavior of species of DEA in the mixture to that of its alone were observed. Whereas, the predicted speciation of piperazine in mixture reflects a slight difference to that of only its carbonated aqueous solution, specifically at low $CO_2$ loadings. The behavior of the PZ species concentration follows a similar behavior to that of MDEA-PZ system. However, in case of DEA the reaction is faster with $CO_2$ to that of MDEA. Generally, the bicarbonate formation gives a high loading of $CO_2$, but due to the little carbamate formation, the reaction kinetics is slow. A free and higher amine concentration relatively counteracts the kinetics that is slow, but the whole rate absorption could be slower than amines that are secondary.

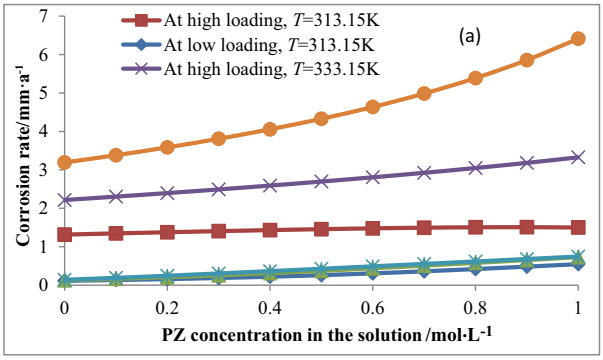


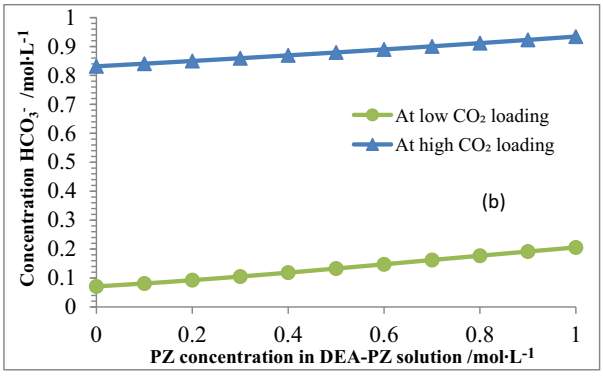


**Fig. 6.** Effect of PZ addition: (a) on the rate of corrosion of carbon steel in solutions of DEA-PZ at low and high $CO_2$ loading. (b) on the concentration of $HCO_3^-$ in the bulk solution of DEA-PZ at 333.15 K.

As seen in Fig. 2, the concentration of bulk of $H_3O^+$, $HCO_3^-$, $DEACOO^-$, $DEAH^+$, $PZH^+$, $PZCOO^-$, $H^+PZCOO^-$ and $PZ(COO^-)_2$ increases with $CO_2$ loading. Nonetheless, $H_3O^+$ and $HCO_3^-$ have higher sensitivity towards the loading of $CO_2$ than PZ and DEA species which show dependence on the amine concentration in the solution. With the common information that corrosion rises with the loading of $CO_2$, this indicates that $H_3O^+$ and $HCO_3^-$ may play a vital role in corrosion. It must be noted that $HCO_3^-$ have more impact on the rate of corrosion than $H_3O^+$ because the $HCO_3^-$ quantity is higher in the solution than $H_3O^+$ (*i.e.* the $HCO_3^-$ concentration is 0.00438 to 1.04 whereas the $H_3O^+$ concentration is $4.6\times10^{-11}$ to $3.2\times10^{-8}$ in the 1.8 mol·L$^{-1}$ DEA + 0.1 mol·L$^{-1}$ PZ).

### 4.2. The corrosion rate of carbon steel in carbonated system of aqueous DEA-PZ

The developed model for the rate of corrosion was applied to model the process of corrosion and to foresee the corrosion rate of carbon steel in carbonated aqueous systems of DEA-PZ. The predicted results through model were compared with those of the experimental results. Comparison have been exhibited through making polarization curves and kinetic data of electrode, current density of corrosion ($i_{corr}$), potential of corrosion ($E_{corr}$), and the corrosion rate, as illustrated in Fig. 3 and Tables 3–6.

A detailed comparison in predicted results against experimental measurements for rate of corrosion is exhibited from Fig. 3 and Tables 3–6. A similar trend has been observed in most of the simulated curves of polarization from the models to that of experimental curves of polarization. However, the simulated curves slightly differ at the bigger current densities direction ($i_{corr}$) and smaller potential of corrosion ($E_{corr}$). This indicates that the predicted rates of corrosion are larger than those of obtained through experiments. The nonconformity of predicted polarization curves may be because of the values of concentration of iron in the bulk solution, which were obtained from [39] as an ionic temperature and strength function. The polarization curves generated from the model have closeness to the experimental curves. The lower rates of corrosion predicted in the system of DEA-PZ from the model due to exchange current density of the values of protonated DEA and protonated PZ used in this model have similarity to protonated MDEA.

### 4.3. Effect of $CO_2$ loading on the corrosion rate

The effect of $CO_2$ loading is shown by comparing the model results with those of experimental measurements in aqueous solutions of DEA-PZ. Fig. 4 shows that $CO_2$ loading has the direct effect on the rate of corrosion on the carbon steel. A high of $CO_2$ loading of the solution has more corrosiveness than that at low $CO_2$ loading. The corrosion rate increases with increase in $CO_2$ loadings of activated systems of DEA (1.9 mol·L$^{-1}$ DEA + 0.05 mol·L$^{-1}$ PZ). The Fig. 4b illustrates that the rate of corrosion rose from 0.42 to 1.72 mm·a$^{-1}$ on increasing the $CO_2$ loading from 0.20 to 0.67 (mol $CO_2$·(mol alkalinity)$^{-1}$). Such rise in the rate of corrosion is because of the increase in dissolved $CO_2$

which forms protonated and bicarbonate diethanolamine ions, which stimulates more dissolution of iron that in turn accelerates the process of corrosion.

Acids react with amine by a transfer reaction of proton due to presence of a free pair of electrons on the nitrogen of amine group. The abundant acidic ions present in the solution react with the metal. In the case of solutions of DEA, Shahid & Faisal [7] reported that $DEAH^+$ ions have more concentration than the hydrogen ions and thus the metal dissolution mechanism for DEA corrosion of solutions can be represented better by the reaction of reduction of $DEAH^+$. Furthermore, increase in the rate of corrosion is attributed to the increase in concentration of $DEAH^+$ ions in the solution; hence, the higher the quantity of $DEAH^+$ ions, the higher will be the iron dissolution leading to more corrosion.

Although the mechanism of corrosion is different in activated DEA and MDEA, both amine systems reflect a rise in the rate of corrosion with rise in the $CO_2$ loading. This is reported to happen because of the concentration of $HCO_3^-$ ions in the system. The bicarbonate ion is the oxidizing agent for the two systems, which are carbonated. Gray *et al.* [40] proposed that the charge transfer that controls the reduction of bicarbonate ion might be the cathodic reaction at a dominant pH of 6 to 10 in corrosion caused by $CO_2$. Hamada *et al.* [41] found that the rate of corrosion of carbon steel in DEA + $K_2CO_3$ solution increases with increasing $CO_2$ loading. They reported that the rate controlling step of corrosion of carbon steel in the solution is the phase diffusion of liquid $HCO_3^-$ across the layer of diffusion formed at the interface of metal-solution. Frolova *et al.* [42] explored bicarbonate ion concentration effect on the rate of corrosion of high and low strength steel in 1 $mol \cdot L^{-1}$ solutions of sodium and carbonate. They found that the rate of corrosion increases with increasing the concentration of bicarbonate. Banks [43] reported that high rate of corrosion in system of carbonate is because of high concentration bicarbonate.

At low $CO_2$ partial pressure, the addition of PZ yields higher amount of $HCO_3^-$, which in turn dissociates due to the increase in $CO_2$ loading, which drives the corrosion process to proceed faster. This causes increase in corrosion rate due to corrosion reaction between iron and bicarbonate as shown in reaction (54) [44].

$$Fe^{2+} + HCO_3^- \rightleftharpoons FeCO_3 + H^+ \quad (54)$$

Carbamate formation takes place when DEA reacts with $CO_2$. The carbamate turns into bicarbonate by hydrolysis based on carbamate reversion reaction of diethanolamine and increasing bicarbonate concentration in the system of DEA-PZ. Similarly, Chakma & Meisen [45] found that at the $CO_2$ partial pressure of 1.38 MPa, the rate of corrosion was 0.61 $mm \cdot a^{-1}$, which increased to 0.8 $mm \cdot a^{-1}$ at $CO_2$ partial pressure of 4.13 MPa.

### 4.4. Effect of temperature on the rate of corrosion

It is obvious that increase in temperature increases the rate of reaction. Based on this theory, the rate of corrosion increase may be predicted when the temperature is increased. The solution temperature effect on the rate of corrosion of carbon steel was examined by simulating six various activated DEA concentrations at different temperatures of solution. For the system of activated DEA low loadings ranged from 0.01 to 0.36 mol of $CO_2$ per mole of alkalinity, while the high loading ranged from 0.17 to 0.77 mol of $CO_2$ per mole alkalinity.

The increase in solution temperature decreases the $CO_2$ loading of activated DEA solutions and thereby reducing the oxidizing agent concentration in the solution. Corrosion depends on oxidizing agent flow to interface of carbon steel solution. The results of corrosion as shown in Fig. 5, reflects that the temperature of solution has a direct relation to the rate of corrosion, a rise in the temperature of solution resulted an increase in the rate of corrosion. This can be indicated by the reaction kinetics dependence on temperature. For high $CO_2$ loading the rate of corrosion of carbon steel increased with increasing temperature. This is because of high carbamate concentration in the solution. The carbamates are the primary cause for the iron chelate formation, which helps to cause the increase in the rate of corrosion, by increasing concentration of oxidizing agent (mainly $HCO_3^-$) in the solution. Primary carbamates of amines form strong chelating agents and can form a chelate soluble compound with $Fe^{2+}$ [46]. Furthermore, because higher viscosity of the fluid that causes the electrochemical species diffusion (which is included in corrosion phenomenon) between the strenuous electrodes. It is predicted that at high $CO_2$ loading and high temperature, the rate of mass transfer of $CO_2$ is affected positively by the driving force that is increased to rise the rate of corrosion in DEA-PZ as illustrated in Fig. 5.

### 4.5. Effect of addition PZ on the rate of corrosion

The effect of addition of PZ on the rate of corrosion of carbon steel was simulated for 2$mol \cdot L^{-1}$ total solution alkalinity for three different temperatures of solution at different $CO_2$ loadings. Results in Fig. 6a reflect that at low $CO_2$ loading the rate of corrosion of carbon steel increased with the increase in concentration of PZ at the three temperatures of solution. The increase in corrosion rate is anticipated to the increase in concentrations of oxidizing agent for the systems. At low partial pressure of $CO_2$ and solution temperature the PZ affected on DEA as an activator to increase the loading of $CO_2$ which increased the $HCO_3^-$ and protonated concentrations of amine in both systems which resulted in rise of the rate of corrosion. Whereas, at high $CO_2$ loading the rate of corrosion of carbon steel increased with the increase in concentration of PZ as illustrated in Fig. 6a. This is because of the increase in $HCO_3^-$ concentration from $CO_2$ that is dissolved, and hydrolysis DEA carbamate as illustrated in Fig. 6b.

## 5. Conclusions

A mechanistic model for corrosion of carbon steel in carbonated aqueous solutions of activated DEA was developed successfully. The use of e-NRTL model to develop rate model for corrosion provided with improved accuracy for prediction of corrosion rate. The carbon steel corrosion rate in activated DEA systems is influenced by $CO_2$ loading, solution temperature and concentration of activator (PZ). Hydronium ion $H_3O^+$ contributed least to the rate of corrosion of carbon steel in activated DEA systems, in comparison to other oxidizing agents ($H_2O$, $HCO_3^-$, $PZH^+$, and $DEAH^+$). The partial contribution of bicarbonate, water reduction, and protonated amine to the rate of corrosion depends on the concentration of activator. At low concentration of activator, protonated and bicarbonate amine reduction contribution are significant in comparison to the water reduction contribution. The order of corrosiveness of carbon steel in aqueous solutions is mainly controlled by their absorption capacity of $CO_2$, where high corrosion rate is found at high $CO_2$ loading. $CO_2$ loading effected on the anodic and cathodic reactions. $HCO_3^-$ reduction is more sensitive to $CO_2$ loading than other oxidizing agents. Temperature of solution changes the iron dissolution kinetics but slightly affects reactions that are cathodic. The deviation between measured and predicted values of $CO_2$ loading is less than 9.81%. Absolute average deviations in experimental and predicted values of corrosion potential and corrosion rates are obtained as 2.77% and 26.36% respectively for 2$mol \cdot L^{-1}$ DEA. Whereas, AAD in experimental and predicted values of corrosion potential and corrosion rates for the blend of DEA and PZ ranged from 1.6% to 2.17% and 17.89% to 39.37% respectively.

## Acknowledgements

Authors gratefully acknowledge the financial support provided by the Ministry of Higher Education & Scientific Research of Iraq.

## Supplementary Material

Supplementary data to this article can be found online at https://doi.org/10.1016/j.cjche.2020.03.006.

## References


[1] S.J. Davis, K. Caldeira, H.D. Matthews, Future $CO_2$ emissions and climate change from existing energy infrastructure, *Science* 329 (2010) 1330–1333.

[2] Z. Zhang, T.N.G. Borhani, M.H. El-Nas, Chapter 4.5 - carbon capture, in: I. Dincer, C.O. Colpan, O. Kizilkan (Eds.), Exergetic, Energetic and Environmental Dimensions, Academic Press 2018, pp. 997–1016.

[3] P. Wattanaphan, Studies and Prevention of Carbon Steel Corrosion and Solvent Degradation during Amine-Based $CO_2$ Capture from Industrial Gas Streams, Ph.D Thesis. Faculty of Graduate Studies and Research, University of Regina, Regina, 2012.

[4] J. Yan, Z. Zhang, Carbon capture, utilization and storage (CCUS), *Appl. Energy* 235 (2019) 1289–1299.

[5] I.M. Saeed, P. Alaba, S.A. Mazari, W.J. Basirun, V.S. Lee, N. Sabzoi, Opportunities and challenges in the development of monoethanolamine and its blends for post-combustion $CO_2$ capture, *Int. J. Greenhouse Gas Control* 79 (2018) 212–233.

[6] S. Rinprasertmeechai, S. Chavadej, P. Rangsunvigit, S. Kulprathipanja, Carbon dioxide removal from flue gas using amine-based hybrid solvent absorption, *Int. J. Chem. Biol. Eng.* 6 (2012) 296–300.

[7] M. Shahid, M. Faisal, Effect of hydrogen sulfide gas concentration on the corrosion behavior of "ASTM A-106 Grade-A" carbon steel in 14% diethanol amine solution, *Arab. J. Sci. Eng.* 34 (2009) 179.

[8] R. Mesgarian, Corrosion Management in Gas Treating Plants (GTP's): Comparison between Corrosion Rate of DEA and MDEA a Case Study in Sour Gas Refinery, International Conference on Industrial Engineering and Operations Management, Bali, Indonesia, 2014.

[9] Z. Zhang, F. Chen, M. Rezakazemi, W. Zhang, C. Lu, H. Chang, X. Quan, Modeling of a $CO_2$-piperazine-membrane absorption system, *Chem. Eng. Res. Des.* 131 (2018) 375–384.

[10] L. Ghalib, B.S. Ali, W.M. Ashri, S. Mazari, I.M. Saeed, Modeling the effect of piperazine on $CO_2$ loading in MDEA/PZ mixture, *Fluid Phase Equilib.* 434 (2017) 233–243.

[11] L. Ghalib, B.S. Ali, W.M. Ashri, S. Mazari, Effect of piperazine on solubility of carbon dioxide using aqueous diethanolamnie, *Fluid Phase Equilib.* 414 (2016) 1–13.

[12] C.T. Liu, K.B. Fischer, G.T. Rochelle, Corrosion by aqueous piperazine at 40–150 °C in pilot testing of $CO_2$ capture, *Ind. Eng. Chem. Res.* 59 (15) (2020) 7189–7197.

[13] L. Zheng, N.S. Matin, J. Landon, G.A. Thomas, K. Liu, $CO_2$ loading-dependent corrosion of carbon steel and formation of corrosion products in anoxic 30 wt.% monoethanolamine-based solutions, *Corros. Sci.* 102 (2016) 44–54.

[14] K. Fischer, G. Rochelle, Fe2+ Solubility and Siderite Formation in Monoethanolamine and Piperazine Solvents, 14th Greenhouse Gas Control Technologies Conference Melbourne, 2018 21–26.

[15] M. Nainar, A. Veawab, Corrosion in $CO_2$ capture process using blended monoethanolamine and piperazine, *Ind. Eng. Chem. Res.* 48 (2009) 9299–9306.

[16] B. Zhao, Y. Sun, Y. Yuan, J. Gao, S. Wang, Y. Zhuo, C. Chen, Study on corrosion in $CO_2$ chemical absorption process using amine solution, *Energy Procedia* 4 (2011) 93–100.

[17] C. Louis, K.L.S. Campbell, D.R. Williams, Carbon steel corrosion in piperazine-promoted blends under $CO_2$ capture conditions, *Int. J. Greenhouse Gas Control* 55 (2016) 144–152.

[18] Y. Xiang, H. Huang, Z. Long, C. Li, W. Yan, Role of residual 2-amino-2-methyl-1-propanol and piperazine in the corrosion of X80 steel within an impure supercritical $CO_2$ environment as relevant to CCUS, *Int. J. Greenhouse Gas Control* 82 (2019) 127–137.

[19] L. Ghalib, B.S. Ali, S. Mazari, W.M. Ashri, I.M. Saeed, Modeling the effect of piperazine on carbon steel corrosion rate in carbonated activated MDEA solutions, *Int. J. Electrochem. Sci.* 11 (2016) 4560–4585.

[20] B.S. Ali, Carbon Dioxide Absorption and its Corrosivity in Aqueous Solutions of Activated Diethanolamine and Methyldiethanolamine and their Mixtures ,Ph.D Thesis, Faculty of Engineering, University of Malaya, Kuala Lumpur, 2007.

[21] S. Bishnoi, G.T. Rochelle, Thermodynamics of piperazine/methyldiethanolamine/water/carbon dioxide, *Ind. Eng. Chem. Res.* 41 (2002) 604–612.

[22] D.M. Austgen, G.T. Rochelle, X. Peng, C.C. Chen, Model of vapor-liquid equilibria for aqueous acid gas-alkanolamine systems using the electrolyte-NRTL equation, *Ind. Eng. Chem. Res.* 28 (1989) 1060–1073.

[23] R. Sidi-Boumedine, S. Horstmann, K. Fischer, E. Provost, W. Fürst, J. Gmehling, Experimental determination of carbon dioxide solubility data in aqueous alkanolamine solutions, *Fluid Phase Equilib.* 218 (2004) 85–94.

[24] M. Haji-Sulaiman, M. Aroua, A. Benamor, Analysis of equilibrium data of $CO_2$ in aqueous solutions of DEA, MDEA and their mixtures using the modified Kent Eisenberg model, *Trans Chem E* 76 (1998) 961–968.

[25] O.F. Dawodu, A. Meisen, Solubility of carbon dioxide in aqueous mixtures of alkanolamines, *J. Chem. Eng. Data* 39 (1994) 548–552.

[26] J.I. Lee, F.D. Otto, A.E. Mather, Solubility of carbon dioxide in aqueous diethanolamine solutions at high pressures, *J. Chem. Eng. Data* 17 (1972) 465–468.

[27] M.K. Mondal, Solubility of carbon dioxide in an aqueous blend of diethanolamine and piperazine, *J. Chem. Eng. Data* 54 (2009) 2381–2385.

[28] B.E. Poling, J.M. Prausnitz, J.P. O'connell, The properties of gases and liquids, McGraw-Hill New York, 2001.

[29] C.F. Spencer, R.P. Danner, Prediction of bubble-point density of mixtures, *J. Chem. Eng. Data* 18 (1973) 230–234.

[30] G. Soave, Equilibrium constants from a modified Redlich-Kwong equation of state, *Chem. Eng. Sci.* 27 (1972) 1197–1203.

[31] C.C. Chen, L.B. Evans, A local composition model for the excess Gibbs energy of aqueous electrolyte systems, *AIChE J.* 32 (1986) 444–454.

[32] B. Mock, L. Evans, C.C. Chen, Thermodynamic representation of phase equilibria of mixed-solvent electrolyte systems, *AIChE J.* 32 (1986) 1655–1664.

[33] H. Renon, J.M. Prausnitz, Local compositions in thermodynamic excess functions for liquid mixtures, *AIChE J.* 14 (1968) 135–144.

[34] K.S. Pitzer, Electrolytes. From dilute solutions to fused salts, *J. Am. Chem. Soc.* 102 (1980) 2902–2906.

[35] V.G. Levich, Physicochemical Hydrodynamics, Prentice-hall Englewood Cliffs, NJ1962.

[36] J.E. Critchfield, $CO_2$ Absorption/Desorption Methyldiethanolamine Solutions Promoted with Monoethanolamine and Diethanolamine: Mass Transfer and Reaction Kinetics, 1988.

[37] R.H. Weiland, J.C. Dingman, D.B. Cronin, G.J. Browning, Density and viscosity of some partially carbonated aqueous alkanolamine solutions and their blends, *J. Chem. Eng. Data* 43 (1998) 378–382.

[38] A. Najumudeen, Development of a Mechanistic Corrosion Model for Carbon Steel in MEA-Based $CO_2$ Absorption Process, Ms. Thesis, University of Regina, Faculty of Graduate Studies and Research, Regina, 2012.

[39] W. Sun, S. Nešić, R.C. Woollam, The effect of temperature and ionic strength on iron carbonate ($FeCO_3$) solubility limit, *Corros. Sci.* 51 (2009) 1273–1276.

[40] L.G. Gray, B.G. Anderson, M.J. Danysh, P.R. Tremaine, Mechanisms of Carbon Steel Corrosion in Brines Containing Dissolved Carbon Dioxide at pH 4, Corrosion/89, Paper, 1989.

[41] M. Hamada, T. Zewail, H. Farag, Study of corrosion behaviour of A106 carbon steel absorber for $CO_2$ removal in amine promoted hot potassium carbonate solution (Benfield solution), *Corros. Eng. Sci. Technol.* 49 (2014) 209–218.

[42] L. Frolova, M. Fokin, V. Zorina, Corrosion-Electrochemical behavior of carbon steels in carbonate-bicarbonate solutions, *Protection of metals.* 33 (3) (1997) 281–284.

[43] W. Banks, Corrosion in hot carbonate systems, *Mater. Prot. Performance.* 6 (1967) 37–41.

[44] D. Davies, G. Burstein, The effects of bicarbonate on the corrosion and passivation of iron, *Corrosion* 36 (1980) 416–422.

[45] A. Chakma, A. Meisen, Corrosivity of diethanolamine solutions and their degradation products, *Ind. Eng. Chem. Prod. Res. Dev.* 25 (1986) 627–630.

[46] Y. Tomoe, K. Sato, Uneven distribution of metallic ions in deposits precipitated in the Koshijihara DGA $CO_2$ removal units in: Corrosion 97, *NACE Int* (1997)339.